ZBP1 promotes RIPK1-dependent apoptosis in aristolochic acid nephropathy

Zhenhuan Zou[1,2,3,#], Keng Ye[1,2,3,#], Fengbin Chen[4], Kongwen Lin[1,2,3], Yankun Song[5], Guoping Li[5], Caiming Chen[1,2,3], Yujia Wang[1,2,3], Huabin Ma[2,6,*], Yanfang Xu[1,2,3,6,*]

[1]Department of Nephrology, Blood Purification Research Center, the First Affiliated Hospital, Fujian Medical University, Fuzhou 350005, China

[2]Research Center for Metabolic Chronic Kidney Disease, the First Affiliated Hospital, Fujian Medical University, Fuzhou 350005, China

[3]Department of Nephrology, National Regional Medical Center, Binhai Campus of the First Affiliated Hospital, Fujian Medical University, Fuzhou 350212, China

[4]Department of Traditional Chinese Medicine, The First Affiliated Hospital, Fujian Medical University, Fuzhou, 350005, China

[5]Department of Pathology, the First Affiliated Hospital, Fujian Medical University, Fuzhou, 350005, China

[6]Central Laboratory, the First Affiliated Hospital, Fujian Medical University, Fuzhou 350005, China

[#]These authors contributed equally: Zhenhuan Zou, Keng Ye

[*]**Correspondence to:**

Science Press

ZR Zoological Research

Yanfang Xu, email: xuyanfang99@hotmail.com; Huabin Ma, email: mahuabin@fjmu.edu.cn

Running title: AA1 induced ZBP1-RIPK1-CASP8 dependent of apoptosis

Science Press
ZR Zoological Research

ABSTRACT

Aristolochic acid nephropathy (AAN) is a progressive form of kidney disease marked by acute tubular injury and interstitial fibrosis, ultimately leading to end-stage renal disease (ESRD). Despite regulatory restrictions, aristolochic acid (AA) remains a global health threat due to its presence in traditional herbal medicines. While mitochondria-mediated apoptosis is a hallmark of AA-induced tubular epithelial cell (TEC) injury, the upstream molecular mechanisms remain unclear. Here, we identify Z-DNA–binding protein 1 (ZBP1) as a key mediator of AA-induced kidney injury. Using *Zbp1* knockout (*Zbp1*$^{-/-}$) and Zα domain–mutant (*Zα*^{Mut}) mice, we show that loss of ZBP1 or its Z-form nucleic acid sensing capability protects against AA-induced renal dysfunction, apoptosis, and inflammation. Mechanistically, aristolochic acid I (AAI) induces mitochondrial oxidative stress and release of mitochondrial DNA (mtDNA), which adopts a Z-conformation and is recognized by ZBP1. The ZBP1 binding subsequently promotes RHIM-dependent interaction with RIPK1, culminating in caspase-8 activation and apoptotic cell death. Notably, ZBP1-mediated cell death was abolished by RIPK1 kinase inhibition or mutation, but unaffected by *Ripk3* or *Mlkl* deletion, revealing a mechanism distinct from RIPK3/MLKL-dependent necroptosis. These findings uncover a previously unrecognized ZBP1–RIPK1–caspase-8 signaling axis driving non-canonical

apoptosis in AAN and suggest that targeting this pathway may provide a novel therapeutic approach for nephrotoxin-induced kidney injury.

KEYWORDS

Aristolochic acid nephropathy; Apoptosis; Mitochondria; ZBP1; Z-DNA

INTRODUCTION

Aristolochic acids (AAs), naturally occurring nitrophenanthrene carboxylic acids found in plants of the *Aristolochia* and *Asarum* genera, are now widely recognized as potent nephrotoxins and carcinogens (Gökmen et al., 2013). Despite regulatory restrictions in many countries, exposure to AAs remains a global health concern due to their continued use in unregulated traditional herbal medicines (Debelle et al., 2008; Jelaković et al., 2015; Kiliś-Pstrusińska and Wiela-Hojeńska, 2021; Yang et al., 2018). Aristolochic acid nephropathy (AAN), first identified in the early 1990s, is a progressive renal disease characterized by acute proximal tubular epithelial cell (TEC) injury, interstitial fibrosis, and a markedly elevated risk of upper urinary tract urothelial carcinoma (Han et al., 2019; Vanherweghem et al., 1993). After cellular uptake via organic anion transporters OAT1 and OAT3, aristolochic acid I (AAI)—the most toxic and abundant AA compound—accumulates in proximal tubular cells, inducing mitochondrial dysfunction, oxidative stress, and the formation of mutagenic DNA adducts (Ji et al., 2021; Shen et al., 2020; Xue et al., 2011).

Apoptosis is a hallmark of AAN pathogenesis, yet its regulation appears context dependent. AAI downregulates anti-apoptotic proteins such as Bcl-2 and Bcl-xL while upregulating the pro-apoptotic protein Bax, leading to mitochondrial membrane depolarization, cytochrome c release, and caspase-3 activation (Pozdzik et al., 2008; Xie et al., 2017). Additionally, AAI

promotes oxidative and endoplasmic reticulum (ER) stress, partly via intracellular Ca^{2+} overload, and activates signaling pathways including p53, STAT3, and MAPKs (Sborchia et al., 2019; Zhou et al., 2010). Pharmacologic inhibition of caspases using the pan-caspase inhibitor Z-VAD-FMK has been shown to attenuate apoptosis induced by AAI in TECs or human bladder RT4 cells (Bellamri et al., 2021; Wang et al., 2024; Wu et al., 2015). However, the upstream molecular sensors that detect AAI-induced mitochondrial and genomic injury and initiate apoptosis execution remain incompletely understood.

Recent studies have highlighted the emerging role of Z-DNA–binding protein 1 (ZBP1; also known as DAI) as a cytosolic nucleic acid sensor that induces regulated cell death and inflammation (Kuriakose and Kanneganti, 2018). ZBP1 contains tandem Zα domains capable of recognizing left-handed Z-form nucleic acids, including viral Z-RNA and endogenous mitochondrial DNA (Z-mtDNA), and a RIP homotypic interaction motif (RHIM) that recruits receptor-interacting protein kinase 3 (RIPK3) to activate MLKL-dependent necroptosis, or RIPK1 to trigger apoptosis via caspase-8 (Jiao et al., 2020; Rodriguez et al., 2022; Solon et al., 2024; Takaoka et al., 2007). RIPK1 serves as a key checkpoint modulating cell fate: it promotes NF-κB–mediated survival and inflammation, or mediates regulated cell death (RCD) by scaffolding FADD–caspase-8 complexes or forming RHIM-dependent necrosomes with RIPK3 and MLKL (Ofengeim and Yuan, 2013; Yuan and Ofengeim, 2024). Crucially, RIPK1

can restrain ZBP1–RIPK3 interactions, and its deletion leads to unrestrained ZBP1-driven necroptosis and inflammation (Koerner et al., 2024; Lin et al., 2016; Newton et al., 2016).

Although ZBP1 has been extensively characterized in antiviral responses and inflammatory diseases, its role in sterile organ injury caused by chemical toxins has only recently begun to emerge (Maelfait and Rehwinkel, 2023). Accumulating evidence suggests that ZBP1 functions as a cytosolic sensor of Z-mtDNA, linking mitochondria damage to regulated cell death pathways. A pivotal study demonstrated that ZBP1, in cooperation with cGAS, senses Z-mtDNA released during doxorubicin-induced mitochondrial damage, thereby promoting cardiomyocyte death and cardiotoxicity (Lei et al., 2023). Our work further demonstrated that ZBP1 detects Z-mtDNA in diquat poisoning or oxalate-induced AKI, triggering RIPK3-dependent necroptosis and ferroptosis (Chen et al., 2025; Lai et al., 2024). Together, these studies reveal a common pathological mechanism in which mitochondrial stress and cytosolic Z-mtDNA release activate ZBP1-driven necroinflammatory pathways across different tissues. However, whether a similar mechanism operates in AAN remains unclear.

In this study, we identify ZBP1 as a critical upstream mediator of non-canonical apoptosis in AAN. We demonstrate that AAI-induced mitochondrial damage results in cytosolic accumulation of Z-mtDNA, which is recognized by ZBP1 through its Zα domain. Activated ZBP1 then engages RIPK1 via RHIM–RHIM interactions, promoting caspase-8 activation and

apoptosis independent of RIPK3 and MLKL. Our findings reveal a previously unrecognized ZBP1–RIPK1–caspase-8 axis that mediates apoptosis in sterile toxic kidney injury. This work provides mechanistic insight into how AAI-induced mitochondrial damage is transduced into apoptosis and highlights ZBP1 as a potential therapeutic target in AAN.

MATERIALS AND METHODS

Mice

All experiments were conducted using male C57BL/6J mice (10–12 weeks old, 24–28 g). *Zbp1*$^{-/-}$, *Ripk3*$^{-/-}$, *Mlkl*$^{-/-}$ mice were kindly provided by Dr. Jiahuai Han (School of Life Sciences, Xiamen University, China) (Yang et al., 2020), and *Zbp1-Zα*^{Mut} (*Zα*^{Mut}; carrying N46A/Y50A/N122A/Y126A mutations) mice were obtained from Prof. Wei Mo (Zhejiang University, China), and RIPK1 kinase dead (*Ripk1*^{K45A}) mice were obtained from Dr. Jianfeng Wu (Xiamen University, China). *Ksp-Cre* transgenic mice were kindly donated by Prof. Hui-Yao Lan (The Chinese University of Hong Kong). *Zbp1*$^{fl/fl}$ mice were procured from GemPharmatech, Nanjing, China. *Vav-iCre* (Strain #: 008610) mice were procured from Jackson Laboratory. Genotyping was performed via tail-snip PCR (Supplementary Figure S8). All mice were housed in a specific pathogen-free facility under a 12-hour light/dark cycle. To induce AKI, a single intraperitoneal injection of AAI (10 mg/kg in DMSO) was administered; control mice received an equivalent volume of saline. Investigators were blinded to group

allocation during outcome assessments, including histology, cell morphology, qPCR, and western blot.

Cell Culture

Primary mouse proximal tubular epithelial cells (TECs) were isolated and cultured as previously described (Xu et al., 2015). To establish the AAN cell model, TECs were treated with aristolochic acid I (AAI) at 40 μg/mL for the indicated durations. Where applicable, cells were pre-treated with the MLKL inhibitor necrosulfonamide (NSA, 5 μM), RIPK3 inhibitor GSK'872 (2 μM), pan-caspase inhibitor Z-VAD-FMK (20 μM), or RIPK1 inhibitor necrostatin-1 (Nec-1, 30 μM) prior to AAI exposure.

HK-2 cells were maintained in DMEM/F12 medium supplemented with 10% FBS, 1% penicillin/streptomycin, and 1× MEM non-essential amino acids, and treated with AAI (40 μg/mL) under standard culture conditions (37°C, 5% CO_2).

HEK293T cells, mouse fibrosarcoma L929 *Ripk1*-KO, *Ripk3*-KO, and *Mlkl*-KO cell lines were kindly provided by Prof. Jiahuai Han and originally obtained from ATCC. These cells were cultured in DMEM supplemented with 10% FBS, 4 mM L-glutamine, 1% penicillin/streptomycin, and 1× MEM non-essential amino acids at 37°C in a humidified 5% CO_2 incubator.

CRISPR-Cas9-Mediated Knockout Cell Lines

To generate *ZBP1*-KO HK-2 cells, lentiviruses encoding Cas9 and sgRNA targeting *ZBP1* (5′-GCCAGAATGGACCCAACAGC-3′) were produced using the pBOBI-Cas9+gRNA-puro system and used to infect HK-2 cells with 10 μg/mL polybrene. Cells were selected using 2 μg/mL puromycin, followed by single-cell cloning via limiting dilution. Successful knockout was confirmed by sequencing and Western blot.

Chemical reagents and antibodies

The following chemical reagents were used: JC-10 (Solarbio, J8050), MitoTracker (C1035), MitoSOX Green (Invitrogen, M36008), propidium iodide (PI; Beyotime, C1352S), DAPI (Beyotime, C1002), Hoechst 33342 (Beyotime, C1022), and DCFH-DA (Beyotime, S0033S). Aristolochic acid I (AAI, TR1736), Z-VAD-FMK (161401-82-7), GSK-872 (1346546-69-7), necrosulfonamide (1360614-48-7), and necrostatin-1 (4311-88-0) were obtained from MedChemExpress.

Primary antibodies used in this study included: anti-ZBP1 (AdipoGen, AG20B-0010), anti-RIPK1 (Cell Signaling Technology [CST], D94C12, 1:1000), anti-phospho-RIPK1 (Ser166) (CST, D8I3A, 1:1000), anti-caspase-3 (CST, 9662S, 1:1000), anti-cleaved caspase-3 (CST, 9661S, 1:1000), anti-caspase-7 (Proteintech, 27155-1-AP, 1:1000), anti-caspase-8 (CST, 4790S, 1:1000), anti-caspase-9 (Abcam, ab202068, 1:1000), anti-α-smooth muscle actin (α-SMA, Sigma, A5228, 1:1000), anti-Z-DNA (Novus,NB100-749, 1:200), and anti-β-actin (Huabio, EM21002, 1:10000). Additional antibodies included: anti-RIPK3 (Abcam, ab62344, 1:1000), anti-phospho-RIPK3 (T231/S232, ab222320, 1:1000), anti-MLKL (ab255747, 1:1000), anti-phospho-MLKL (S345, ab208910, 1:1000), anti-TOMM20 (ab56783, 1:200),

anti-collagen I (ab34710, 1:200), anti-F4/80 (ab6640, 1:200), anti-Ly6G (ab25377, 1:200), anti-megalin (ab184676, 1:200), and secondary antibodies (Abcam): goat anti-mouse IgG H&L Alexa Fluor® 488 (ab150113, 1:1000), Alexa Fluor® 594 (ab150116, 1:1000); goat anti-rat IgG H&L Alexa Fluor® 568 (1:1000); goat anti-rabbit IgG H&L Alexa Fluor® 568 (1:1000); and donkey anti-sheep IgG H&L Alexa Fluor® 488 (ab150177, 1:1000).

Plasmid Construction

ZBP1 and its mutants (ΔRHIM, $Z\alpha^{Mut}$) were constructed as described in our earlier publication (Lai et al., 2024). RIPK1 (K45A, R588E, RHIM) mutants were generated by two-step PCR amplification using specific primers. The resulting fragments were cloned into BamHI/XhoI sites of pBOB vectors with or without Flag/HA tags. Exo III-assisted ligation-independent cloning was used, and constructs were verified by DNA sequencing.

Lentivirus Production and Infection

Lentiviral particles were generated by co-transfecting HEK293T cells with packaging plasmids (VSVG, PMDL, REV) and pBOB expression constructs (wild-type or mutant cDNAs) using calcium phosphate transfection. Viral supernatants were collected 48 h post-transfection and used to infect target cells in the presence of 10 μg/mL polybrene, followed by centrifugation at 2,500 rpm for 30 minutes at 37°C. After 12 hours, medium was replaced with fresh culture medium. Infected cells were used for experiments 48–60 hours post-infection.

Lentiviral shRNA Knockdown

shRNA oligonucleotides were designed and inserted into the pLV-1 H-EF1a-puro vector using Biosettia's single oligonucleotide RNAi system. Lentiviral particles were produced and used according to standard protocols. shRNA sequences targeting RIPK1 included (Xu et al., 2015):

sh-RIP1 #1: AAAAgcctgagaatatcctcgttTTGGATCCAAaacgaggatattctcaggc

sh-RIP1 #2: AAAAccactagtctgactgatgaTTGGATCCAAtcatcagtcagactagtgg

Quantitative real-time PCR (qRT-PCR)

Total RNA was extracted from kidney tissues using TRIzol™ reagent (Invitrogen). cDNA synthesis was performed using HiScript III All-in-One RT SuperMix (Vazyme, R333-01). qRT-PCR was conducted using 2× Taq Pro Universal SYBR qPCR Master Mix (Vazyme) on a QuantStudio™ 5 Real-Time PCR System. The following primers were used:

(1) *Tnfa*-F: AACTAGTGGTGCCAGCCGAT, *Tnfa*-R: CTTCACAGAGCAATGACTCC;

(2) *IL6*-F: TAGTCCTTCCTACCCCAATTTCC, *IL6*-R: TTGGTCCTTAGCCACTCCTTC;

(3) *IL1b*-F: GGAGAGTGTGGATCCCAAG, *IL1b*-R: GGTGCTGATGTACCAGTTGG;

(4) β-actin-F: GGCTGTATTCCCCTCCATCG, β-actin-R: CCAGTTGGTAACAATGCCATGT;

Flow Cytometry Analysis

Flow cytometry was used to analyze immune cell subtypes in injured kidneys following AAI treatment. Briefly, kidneys were harvested, finely minced, and digested with 1 mg/mL collagenase type IV (Sigma, 11088858001) and DNase I (Thermo Fisher Scientific, 90083) in DMEM at 37 °C for 30 minutes with agitation. The digestion was halted by adding DMEM supplemented with fetal bovine serum (FBS; WISENT, 085-150). The resulting cell suspension was passed through a 40 μm cell strainer, washed with PBS, and subjected to density gradient centrifugation using 40% and 70% Percoll (GE Healthcare, 17-0891-02). The mononuclear cells were collected from the interphase, washed, and resuspended in PBS for flow cytometric staining.

For surface staining, cells were blocked and incubated for 30 minutes at 4 °C with the following antibodies: anti-mouse CD45 (APC-eFluor™ 780, eBioscience™, 47-0451-82) to identify total leukocytes, anti-mouse Ly6G/Ly6C (FITC, eBioscience™, 11-5931-82) for neutrophils ($CD45^+Ly6G^+$), and anti-mouse F4/80 (PE, eBioscience™, 48-4801-82) for macrophages ($CD45^+F4/80^+$). To differentiate macrophage subtypes, anti-mouse CD206 (PE, eBioscience™, 12-2061-82) and anti-mouse iNOS (PB450, eBioscience™, 404-5920-82) were used for M2 and M1 macrophage detection, respectively. Data were acquired using a CytoFLEX B53015 flow cytometer (Beckman).

Lactate Dehydrogenase (LDH) Release Assay

WT and *Zbp1*-KO TECs were seeded and treated as described in the "Cell Culture" section. After treatment, the culture medium was collected and centrifuged at 400 × g for 5 minutes. A 120 μL aliquot of the supernatant was mixed with 60 μL of detection reagent from the LDH Cytotoxicity Assay Kit (Beyotime), incubated in the dark, and the absorbance was measured at 490 nm to assess LDH activity.

Enzyme-Linked Immunosorbent Assay (ELISA)

Following treatment, culture supernatants from WT and *Zbp1*-KO TECs were collected by centrifugation (400 × g, 5 min). The levels of TNF-α (Huabio, EM0010), IL-6 (Huabio, EM0004), and HMGB1 (Animaluni, LV30652) were quantified using ELISA kits according to the manufacturers' instructions.

Assessment of Mitochondrial ROS and Membrane Potential

To measure mitochondrial ROS, AAI-exposed TECs were incubated with 10 μM DCFH-DA, 1 μM MitoTracker, or 1 μM MitoSOX for 30 minutes at 37°C. Cells were washed twice with

HBSS and visualized using a ZEISS LSM800 confocal microscope. Mitochondrial membrane potential (MMP) was assessed using the JC-10 staining kit. Cells were stained with 10 μM JC-10 for 30 minutes at 37°C, following the manufacturer's protocol (Solarbio, J8050), and images were acquired using confocal microscopy.

Western blot

Western blotting was performed as previously described (Xu et al., 2015). Briefly, proteins from kidney tissues, TECs, and HK-2 cells were extracted, quantified, denatured, separated by SDS-PAGE, and transferred to PVDF membranes. After blocking and antibody incubation, signals were detected using enhanced chemiluminescence (ECL).

Immunoprecipitation

TECs, or HEK293T cells were harvested after indicated treatment and lysed in PBS containing 1% Triton X-100, protease, and phosphatase inhibitors (New Cell & Molecular Biotech, P002). Lysates were incubated on ice for 10 minutes, thensonicated (1s on, 3s off, 20% power) for 2 minutes. After centrifugation (12,000 rpm, 30 min), the supernatants were incubated with anti-RIPK1 antibody and protein A/G beads, or anti-Flag (Abmart, M20018) agarose-conjugated beads at 4°C for 6 hours. Beads were washed and bound proteins were subsequently eluted using 200 μg/mL 3×Flag peptide in PBS (Beyotime, P9801), followed by boiling with 2× SDS buffer for western blot analysis.

Immunofluorescence staining

Kidney sections were deparaffinized and underwent heat-induced antigen retrieval using citrate buffer. After blocking with 3% BSA for 1 hour, sections were incubated with primary antibodies overnight at 4°C, followed by fluorophore-conjugated secondary antibodies at room temperature for 1 hour in the dark. Cultured TECs were similarly fixed, permeabilized, blocked, and stained. Nuclei were counterstained with DAPI (Beyotime, C1002) for 15 minutes. Images were acquired using a ZEISS LSM800 confocal microscope.

Histological analysis

Kidneys were fixed in paraffin and subjected to periodic acid–Schiff (PAS) and Masson's trichrome staining to assess tubular injury and fibrosis. TUNEL staining was performed using the ApopTag Fluorescein In Situ Apoptosis Detection Kit (Millipore) according to the manufacturer's instructions.

Human samples

A 70-year-old male patient presented with oliguria, generalized edema, and loss of appetite. His serum creatinine levels rose sharply from 0.96 mg/dL to 10.31 mg/dL over six days, indicating acute kidney injury (AKI) following a two-week intake of traditional Chinese medicine containing aristolochic acid. A renal biopsy performed on day 10 revealed prominent granular and vacuolar degeneration of tubular epithelial cells, with associated brush border loss. Eosinophilic casts and red blood cell casts were present within the tubular lumens,

accompanied by interstitial infiltration of lymphocytes and monocytes, consistent with severe tubular injury (Supplementary Figure S4). The Ethics Review Form from the Branch for Medical Research and Clinical Technology Application, Ethics Committee of the First Affiliated Hospital of Fujian Medical University approved the participation of patients in this study (approval number [2024]080).

Statistical Analysis

All experiments were performed at least in triplicate. Data are presented as mean ± standard deviation (SD). Statistical analyses were conducted using GraphPad Prism (v9.5) and IBM SPSS Statistics (v20.0). Group comparisons were made using unpaired two-tailed t-tests. One-way ANOVA followed by Bonferroni post hoc tests was used for multiple group comparisons. A p-value of $P < 0.05$ was considered statistically significant (*$P < 0.05$, **$P < 0.01$, ***$P < 0.001$, ****$P < 0.0001$).

RESULTS

ZBP1 deficiency alleviates aristolochic acid I–induced acute kidney injury

To determine the role of ZBP1 in acute kidney injury (AKI) induced by aristolochic acid I (AAI)(Miao et al., 2024), we administered a single intraperitoneal dose of AAI (10 mg/kg) to wild-type (*Zbp1*$^{+/+}$) and *Zbp1*-deficient (*Zbp1*$^{-/-}$) mice and assessed kidney injury on days 0, 1 and 3 post-injections. Serum biochemical analysis revealed that *Zbp1*$^{-/-}$ mice exhibited

significantly lower levels of serum creatinine and blood urea nitrogen (BUN) compared with their wild-type littermate controls (Figure 1A–B), indicating the preservation of renal function. Histological evaluation of kidney sections stained with periodic acid–Schiff (PAS) demonstrated widespread tubular injury in *Zbp1*$^{+/+}$ mice, including epithelial cell sloughing, cast formation, and luminal obstruction, particularly on day 3 post-injury. In contrast, these pathological changes were markedly attenuated in *Zbp1*$^{-/-}$ mice (Figure 1C). Quantification of tubular injury scores confirmed a ~50% reduction in damage in the *Zbp1*$^{-/-}$ group (Figure 1D). Terminal deoxynucleotidyl transferase dUTP nick-end labeling (TUNEL) staining revealed a substantial decrease in tubular cell death in *Zbp1*$^{-/-}$ kidneys compared with *Zbp1*$^{+/+}$ controls (Figure 1E–F). Furthermore, to confirm the occurrence of apoptosis, we performed immunofluorescence staining for cleaved caspase-3 (cl-C3). Consistently, cl-C3 signals were markedly increased in the kidneys of WT mice after AAI treatment but were significantly attenuated in ZBP1-deficient mice (Supplementary Figure S1). In line with these findings, western blot analysis demonstrated elevated ZBP1 expression in *Zbp1*$^{+/+}$ kidneys, accompanied by increased levels of the injury markers KIM-1 and NGAL following AAI administration, whereas these responses were markedly attenuated in *Zbp1*$^{-/-}$ mice (Figure 1G).

Together, these data indicate that ZBP1 contributes to the development of AAI-induced AKI and that its genetic ablation confers significant protection against both structural and functional kidney injury.

Deletion of *Zbp1* attenuates renal fibrosis following aristolochic acid exposure

To determine whether ZBP1 also contributes to chronic kidney injury (Baudoux et al., 2022), we assessed renal fibrosis on day 14 and day 28 following AAI administration in *Zbp1*$^{+/+}$ and *Zbp1*$^{-/-}$ mice. Masson's trichrome staining of kidney sections revealed extensive interstitial collagen deposition in wild-type mice, whereas *Zbp1*$^{-/-}$ mice exhibited markedly reduced fibrosis (Figure 2A). Morphometric quantification analysis confirmed over 30% reduction in fibrotic area in *Zbp1*$^{-/-}$ kidneys at day 28 (Figure 2B), which paralleled improved renal function, as evidenced by significantly lower serum creatinine and BUN levels compared with *Zbp1*$^{+/+}$ littermates (Figure 2C-D). To further evaluate fibrogenic activation, western blot analysis demonstrated decreased expression of α–smooth muscle actin (α-SMA) and type I collagen (Col I) in *Zbp1*$^{-/-}$ kidneys (Figure 2E). Immunofluorescence staining confirmed fewer α-SMA^{+} myofibroblasts and decreased interstitial collagen I accumulation in *Zbp1*-deficient mice (Figure 2F–I).

These findings suggest that ZBP1 not only exacerbates acute tubular injury but also promotes the fibrotic remodeling that underlies the transition from AKI to chronic kidney disease (CKD) in the setting of AAI exposure.

Absence of ZBP1 suppresses renal inflammation in aristolochic acid–induced nephropathy

Given the well-established role of inflammation in the pathogenesis of AAI-induced kidney injury (Chen et al., 2022), we next evaluated the impact of *Zbp1* deletion on immune cell infiltration and cytokine responses. Immunofluorescence staining of kidney sections from mice treated with AAI revealed substantial interstitial accumulation of $F4/80^+$ macrophages and $Ly6G^+$ neutrophils in $Zbp1^{+/+}$ kidneys. In contrast, immune cell infiltration was markedly reduced in $Zbp1^{-/-}$ kidneys (Figure 3A-B). Quantitative analysis confirmed significant reductions in both $F4/80^+$ and $Ly6G^+$ areas in the absence of ZBP1 (Figure 3C–D). In vehicle-treated control mice, immune cell infiltration was negligible in both genotypes.

To evaluate the inflammatory cytokine milieu, we performed qRT-PCR to quantify renal mRNA levels of TNF-α, IL-6, and IL-1β at days 1, 3, and 7 following AAI administration. In $Zbp1^{+/+}$ mice, expression of these cytokines markedly increased and peaked at day 3. In contrast, this inflammatory response was significantly attenuated in the kidneys of $Zbp1^{-/-}$mice (Figure 3E). Flow cytometric profiling of kidney immune populations revealed genotype-dependent

differences in myeloid cell dynamics. In wild-type mice, the proportions of Ly6G$^+$ neutrophils and iNOS$^+$ M1-like macrophages peaked at day 7 and remained elevated through day 28. *Zbp1*$^{-/-}$ kidneys displayed significantly attenuated accumulation of these pro-inflammatory subsets throughout the time course (Figure 3F-G). Interestingly, while CD206$^+$ M2-like macrophages progressively increased in *Zbp1*$^{+/+}$ mice, surpassing 70% by day 28, their expansion was limited in *Zbp1*$^{-/-}$ kidneys, where CD206$^+$ cells plateaued at approximately 25% (Figure 3H).

Collectively, these data suggest that ZBP1 promotes early recruitment of pro-inflammatory myeloid cells and expansion of reparative macrophage populations in AAI nephropathy. To explicitly address whether these effects are cell-autonomous or secondary to reduced tubular injury, we first examined ZBP1 expression at different time points in AAI-induced acute kidney injury and chronic fibrosis models. Immunofluorescence staining of kidney sections revealed a progressive induction of tubular ZBP1 expression in *Zbp1*$^{+/+}$ mice, which colocalized with SLC22A6, a marker of proximal tubular cells (Supplementary Figure S2). Subsequently, tubular epithelial cell–specific *Zbp1* (*Zbp1*$^{fl/fl}$; *Ksp*^{Cre}) and hematopoietic cell–specific *Zbp1* (*Zbp1*$^{fl/fl}$; *Vav*^{Cre}) knockout mice were generated and subjected to AAI-induced AAN. Deletion of *Zbp1* in tubular epithelial cells markedly protected against AAI-induced kidney injury, recapitulating the phenotype of global *Zbp1* knockout mice, whereas deletion of *Zbp1* in

hematopoietic cells failed to confer protection at early stage (d1-d3), but mitigated renal injury at later stage (Supplementary Figure S3). These findings indicate that ZBP1 primarily functions within tubular epithelial cells rather than immune cells. Moreover, *Zbp1* deletion had no effect on NF-κB activation (Fig. 1G), suggesting that the reduced inflammation in *Zbp1*-deficient mice is secondary to decreased tubular cell death rather than a direct suppression of inflammatory signaling.

ZBP1 promotes tubular epithelial cell death and inflammatory responses upon AAI exposure *in vitro*

To delineate the cell-intrinsic role of ZBP1 in tubular injury, we analyzed cell death and inflammatory responses in primary tubular epithelial cells (TECs) isolated from *Zbp1*$^{+/+}$ and *Zbp1*$^{-/-}$ mice. Time-lapse live-cell imaging demonstrated that the annexin V^{+}/PI^{-} cells appeared as early as 6 hours after AAI exposure, indicating early apoptosis, whereas PI^{+} cells emerged at 12 hours, indicating subsequent secondary necrosis (Figure 4A-B). Notably, this effect was substantially attenuated in *Zbp1*$^{-/-}$ cells (Figure 4A-B). In line with this, measurement of lactate dehydrogenase (LDH) release—an indicator of plasma membrane rupture—also showed a marked reduction in *Zbp1*-deficient cells (Figure 4C). In addition, ELISA analysis of culture supernatants revealed that AAI treatment induced a time-dependent increase in the release of IL-6, TNF-α, and HMGB1 in *Zbp1*$^{+/+}$ TECs, all of which were significantly reduced in *Zbp1*$^{-/-}$ cells (Figure 4D–F).

To validate these findings in a human context, CRISPR/Cas9-mediated knockout of *ZBP1* was performed in HK-2 cells, introducing a 10- base pair deletion in exon 1 (Figure 4G). Western blot confirmed effective depletion of ZBP1 protein (Figure 4H). Upon AAI stimulation, *ZBP1*-knockout HK-2 cells showed significantly reduced PI positivity at 18 and 24 hours compared with wild-type controls (Figure 4I–J). ATP-based viability assays further demonstrated improved cell survival in the absence of *ZBP1* (Figure 4K).

Together, these *in vitro* results indicate that ZBP1 plays a central role in mediating both tubular epithelial cell death and the associated inflammatory response during AAI-induced injury.

AAI induces mitochondrial stress, cytosolic mtDNA leakage, and Z-DNA formation that colocalizes with ZBP1

To elucidate the upstream signals responsible for ZBP1 activation during AAI-induced injury, we examined mitochondrial integrity and nucleic acid stress in tubular epithelial cells. DCFDA staining revealed a remarkable increase in intracellular reactive oxygen species (ROS) following AAI treatment (Figure 5A). JC-10 staining showed a pronounced shift from red to green fluorescence, indicating mitochondrial membrane depolarization (Figure 5B, D). MitoSOX staining further confirmed elevated mitochondrial superoxide levels in AAI-treated cells (Figure 5C, E). Consistent with mitochondrial damage, confocal microscopy showed

substantial disruption of the mitochondrial network, evidenced by altered Tom20 immunostaining. Importantly, AAI exposure led to robust induction of Z-DNA within the cytoplasm (Figure 5F), which colocalized with ZBP1 in tubular epithelial cells (Figure 5G). *In vivo*, similar colocalization of ZBP1, Tom20, and Z-DNA was observed in renal tubular cells from AAI-treated kidneys (Figure 5H-I). Notably, ZBP1 and Z-DNA colocalization was also observed in renal biopsies from patients with aristolochic acid nephropathy, highlighting the clinical relevance of this signaling axis (Figure 5J; Supplementary Figure S4). To determine whether this response involved the release of mitochondrial DNA (mtDNA) into the cytosol, we quantified both total and cytosolic mtDNA levels. Although total cellular mtDNA content was reduced, consistent with AAI-induced mitochondrial damage (Figure 5K), cytosolic mtDNA levels were significantly elevated upon AAI exposure (Figure 5L), indicating the leakage of mitochondrial components into the cytoplasm.

Taken together, these findings indicate that AAI induces mitochondrial oxidative stress and mtDNA release, which leads to an increased cytoplasmic population of Z-form DNA. This Z-DNA colocalizes with ZBP1 and likely serves as its endogenous ligand in the context of nephrotoxic injury.

The Zα domain of ZBP1 is essential for sensing Z-form DNA and mediates tubular cell death and nephropathy

Given that AAI exposure induces cytosolic accumulation of Z-form mitochondrial DNA (Z-mtDNA), we hypothesized that ZBP1 mediates cell death through its Zα domain, which specifically recognizes Z-DNA. To test this, *Zbp1*$^{-/-}$ TECs were reconstituted with either wild-type ZBP1 or a Zα domain mutant construct (Zα^{Mut}) deficient in Z-DNA binding. Zα^{Mut} failed to restore AAI-induced cell death, as indicated by significantly reduced propidium iodide (PI) uptake compared with cells expressing wild-type ZBP1, despite comparable protein expression levels (Figure 6A–C). To further assess the functional importance of Zα *in vivo*, we employed knock-in mice harboring Zα domain mutations (*Zα*^{Mut}). Time-lapse imaging revealed that TECs derived from *Zα*^{Mut} mice were resistant to AAI-induced cell death, closely resembling the phenotype of *Zbp1*$^{-/-}$ TECs (Figure 6D–E; 4A–B).

We next examined the contribution of the Zα domain to renal injury in the AAN model. Compared to wild-type (WT) littermates, *Zα*^{Mut} mice exhibited significantly lower serum creatinine and blood urea nitrogen (BUN) levels at both early (days 1 and 3) and late (days 14 and 28) phases after AAI administration (Figure 6F–G). Histological analyses further demonstrated markedly attenuated tubular injury and interstitial fibrosis in *Zα*^{Mut} kidneys, as assessed by PAS and Masson' s trichrome staining (Supplementary Figure S5A–D).

Collectively, these findings demonstrate that the Zα domain is indispensable for ZBP1 to sense AAI-induced Z-DNA and initiate tubular epithelial cell death and nephropathy.

ZBP1 interacts with RIPK1 to drive caspase-dependent apoptosis in AAI-induced nephropathy

Building upon the observation that the RHIM domain of ZBP1 is essential for AAI-induced cell death (Figure 6A–C), we next investigated whether the RHIM-dependent ZBP1–RIPK1/RIPK3 signaling axis contributes to the cellular response to AAI. Time-course western blot analysis of renal tissues revealed a robust induction of phosphorylated RIPK1 in wild-type kidneys following AAI administration, which was markedly diminished in both *Zbp1*$^{-/-}$ and *Zα*^{Mut} mice. In contrast, the phosphorylation levels of RIPK3 and MLKL remained comparable across all genotypes (Figure 6H), consistent with the observation that RIPK3 or MLKL deficiency failed to confer protection against AAI-induced AKI (Supplementary Figure S6A–F). These findings suggest that ZBP1-dependent RIPK1 activation occurs independently of the canonical RIPK3–MLKL necroptotic pathway.

Next, we sought to determine how the ZBP1–RIPK1 interaction mediates downstream cell death signaling. Firstly, we found that AAI-induced primary tubular cell death was significantly suppressed by the pan-caspase inhibitor Z-VAD-FMK and the RIPK1 kinase inhibitor necrostatin-1 (Nec-1), but not by the RIPK3 inhibitor GSK'872 or the MLKL inhibitor necrosulfonamide (NSA) (Supplementary Figure S7A–B). Consistently, knockdown of *Ripk1* markedly reduced AAI-induced cell death in primary TECs (Supplementary Figure S7C–E),

whereas neither *Ripk3* nor *Mlkl* knockout provided no protection (Supplementary Figure S7C–G). Likewise, *Ripk1*$^{-/-}$ L929 cells were resistant to AAI, while *Ripk3*$^{-/-}$ and *Mlkl*$^{-/-}$ cells remained susceptible (Supplementary Figure S7H–I). Reconstitution of *Ripk1*$^{-/-}$ L929 cells revealed that wild-type RIPK1—but not RHIM-deleted, kinase-dead (K45A), or death-domain mutants—restored AAI sensitivity (Supplementary Figure S7J–L), demonstrating that RIPK1 kinase activity, RHIM and death domains are all required for this pathway.

To further validate the essential role of RIPK1 kinase activity in AAI-induced kidney injury, RIPK1 kinase-dead (*Ripk1*^{K45A}) mice were subjected to the AAN model, and primary TECs from these mice were analyzed *in vitro*. Notably, *Ripk1*^{K45A} TECs showed significant resistance to AAI-induced apoptosis and secondary necrosis (Fig.7A-B). In addition, *Ripk1*^{K45A} mice exhibited markedly reduced renal injury and fibrosis (Fig. 7C-F). These results provide direct genetic evidence that RIPK1 kinase activity is essential for driving AAI-induced TECs apoptosis and nephropathy.

Finally, we delineated the downstream apoptotic machinery. Western blot analysis over a time course demonstrated that AAI treatment induced sequential cleavage of caspase-8 and caspase-3 in wild-type TECs, whereas this cleavage was markedly diminished in *Zbp1*$^{-/-}$ cells (Figure 7G), supporting the notion that a ZBP1-RIPK1-caspase-8/3 axis is activated specifically. To validate the physical interactions among these proteins, immunoprecipitation assays were performed in TECs following AAI treatment. RIPK1 was found to co-immunoprecipitate with ZBP1 and caspase-8 in a time-dependent manner, indicating the formation of an apoptotic signaling complex (Figure 7H). Importantly, ZBP1 lacking the RHIM

domain failed to recruit either RIPK1 or caspase-8 (Figure 7I), confirming that RHIM-mediated complex formation is required for apoptotic signal transduction.

Collectively, these data define a non-canonical cell death pathway in AAI nephropathy, in which ZBP1 activates RIPK1 via RHIM–RHIM interaction, leading to caspase-8–dependent apoptosis independently of RIPK3 or MLKL.

DISCUSSION

This study uncovers a previously unrecognized mechanism by which Z-DNA–binding protein 1 (ZBP1) orchestrates caspase-8–dependent apoptosis in aristolochic acid nephropathy (AAN), independent of the canonical necroptotic mediators RIPK3 and MLKL. Our data position ZBP1 as a critical upstream sensor of mitochondrial damage–associated Z-form nucleic acids that couples toxic mitochondrial stress to apoptotic cell death signaling via RIPK1. These findings extend the functional repertoire of ZBP1 beyond its established role in antiviral immunity and necroptosis and highlight a broader relevance of ZBP1-driven responses in sterile organ injury.

A defining feature of AAN is the prominent and persistent apoptosis of tubular epithelial cells (TECs) (Pozdzik et al., 2008). While the involvement of mitochondria in initiating apoptotic signaling in AAN is well documented, the upstream molecular events that transduce mitochondrial damage into regulated cell death have remained elusive (Liu et al., 2020; Zhou

et al., 2024). Here, we demonstrate that ZBP1 directly mediates this process by sensing cytosolic mitochondrial DNA (mtDNA) that adopts the left-handed Z-conformation—a structural signature of nucleic acid stress. ZBP1 engagement of Z-mtDNA leads to RHIM-dependent recruitment of RIPK1, promoting caspase-8 activation and apoptotic execution. Notably, this apoptotic program proceeds independently of RIPK3 or MLKL, underscoring a non-canonical ZBP1–RIPK1 axis that is functionally distinct from previously described necroptotic pathways.

ZBP1 is classically recognized as a cytosolic sensor of Z-form nucleic acids that activates necroptosis through its RHIM-mediated interaction with RIPK3, leading to MLKL phosphorylation and membrane rupture (Chen et al., 2025; Lei et al., 2023; Mishra et al., 2025). However, accumulating evidence indicates that ZBP1 is not restricted to the canonical RIPK3–MLKL pathway. ZBP1 can also engage RIPK1 via its RHIM domain to trigger caspase-8–dependent apoptosis or mixed PANoptotic cell death, depending on the cellular context (Koerner et al., 2024; Lin et al., 2016; Muendlein et al., 2021; Newton et al., 2016). In this study, we reveal that in the setting of sterile kidney injury, ZBP1 adopts a distinct function by interacting with RIPK1 to initiate caspase-8–mediated apoptosis. This shift underscores the contextual plasticity of ZBP1, which appears capable of toggling between necroptotic and apoptotic outputs depending on the nature of the upstream stimuli and the cellular environment.

AAI exposure leads to the upregulation of ZBP1 in renal tubular cells, likely driven by both direct nephrotoxic stress and the concomitant induction of type I/II interferon responses, as previously reported (Long et al., 2025; Sasaki et al., 2022). In agreement, we observed a significant increase in ZBP1 expression following AAI administration, preceding overt mitochondrial injury. Since AAI is known to cause mitochondrial damage and mtDNA leakage, we hypothesized that cytosolic mtDNA—specifically in the Z-conformation—acts as a trigger for ZBP1 activation. Indeed, our imaging and functional assays support the notion that Z-form mtDNA accumulation in the cytoplasm activates ZBP1 and initiates the apoptotic cascade.

In vivo, *Zbp1* deletion conferred substantial protection from AAI-induced renal dysfunction, tubular injury, and interstitial inflammation. These protective effects were recapitulated in vitro using primary TECs derived from *Zbp1* knockout mice and cells expressing domain-specific ZBP1 mutants. Disruption of the Zα1 domain or introduction of point mutations that impair Z-DNA binding abolished the pro-apoptotic activity of ZBP1, highlighting the critical role of nucleic acid sensing in this process. This aligns with emerging studies demonstrating that the Zα domains of ZBP1 are indispensable for detecting cytoplasmic Z-nucleic acids and initiating downstream signaling (Ha et al., 2008; Maelfait et al., 2017).

Mechanistically, ZBP1-mediated apoptosis depended on both the scaffold and kinase functions of RIPK1. *Ripk1*^{K45A} mice exhibited markedly reduced renal injury and fibrosis, and

tubular epithelial cells (TECs) derived from these mice showed significant resistance to AAI-induced apoptosis, providing direct genetic evidence that RIPK1 kinase activity is essential for AAI-induced tubular apoptosis and nephropathy. Consistently, complementation experiments demonstrated that both the RHIM and death domains of RIPK1 are indispensable for executing ZBP1-dependent apoptosis. However, neither RIPK3 nor MLKL was activated in this model, and their genetic ablation failed to influence cell death outcomes and kidney injury progression, confirming that necroptosis is dispensable in AAN. These data define a ZBP1–RIPK1–caspase-8 axis that orchestrates apoptosis independently of the canonical necroptotic machinery.

In addition to promoting cell death, ZBP1 deficiency also mitigated AAI-induced inflammation and inflammatory cell infiltration in the kidney. Conditional deletion of *Zbp1* in tubular epithelial cells (*Zbp1*$^{fl/fl}$; *Ksp*^{Cre}) markedly protected against AAI-induced kidney injury, whereas deletion of *Zbp1* in hematopoietic cells (*Zbp1*$^{fl/fl}$; *Vav*^{Cre}) failed to confer protection during the early phase (days 1–3) but ameliorated renal injury at later stages. These findings indicate that the protective effect of ZBP1 deficiency is largely cell-autonomous within TECs, and that its modulation of renal inflammation likely results from reduced release of cell death–associated DAMPs or altered innate immune signaling downstream of cytosolic nucleic acid recognition.

Several limitations should be acknowledged. Although our genetic and imaging data strongly support the involvement of Z-mtDNA in activating ZBP1, direct biochemical evidence of ZBP1 binding to Z-form mtDNA remains to be established. Future studies employing high-resolution structural approaches or crosslinking immunoprecipitation could further delineate this

interaction. Additionally, while our focus was on cell death, ZBP1 may also influence inflammatory gene expression or innate immune receptor signaling, which warrants further investigation. Finally, although acute kidney injury (AKI) is clinically more prevalent in men and our experiments were performed in male mice, further studies involving female animals and additional clinical AAN samples, including those from women, are warranted to determine whether the observed mechanisms are sex-specific (Bao et al., 2018; Chesnaye et al., 2024; Patidar et al., 2025).

In conclusion, we identify a novel ZBP1–RIPK1–caspase-8 signaling axis that drives apoptosis in AAN independently of RIPK3 and MLKL. This mechanism expands the functional repertoire of ZBP1 beyond necroptosis and establishes its role in sensing endogenous Z-form nucleic acids during sterile mitochondrial stress (Figure 8). Targeting the ZBP1–RIPK1–caspase-8 axis—particularly the Zα domains—may represent a promising therapeutic strategy for mitigating nephrotoxin-induced acute kidney injury and its progression to chronic kidney disease.

COMPETING INTERESTS

The authors declare no competing interests.

AUTHOR CONTRIBUTIONS

Y.X., H.M. designed research. Z.Z., K.Y., B.C., K.L., Y.S, G.L., C.C., Y.W. performed the mice and molecular experiments. H.M. and Y.X. wrote the draft manuscript, supervised the research and performed writing-review and editing. All authors read and approved the final version of the manuscript.

ACKNOWLEDGEMENTS

We are grateful to Prof. Jiahuai Han (Xiamen University), Wei Mo (Zhejiang University) for experimental materials. Yanfang Xu was supported by Fujian Research and Training Grants for Young and Middle-aged Leaders in Healthcare (2022QNRCYX-XYF).

FUNDING

This work was supported by grants from National Natural Science Foundation of China (U23A20410, 82470710), Young and Middle-aged Scientific Research Major Project of Fujian Provincial Health Commission (No. 2021ZQNZD004), Program of the First Affiliated Hospital of Fujian Medical University (YJRC4104).

ETHICS APPROVAL AND CONSENT TO PARTICIPATE

The animal experiments were accomplished in compliance with ethical standards. All animal experiments were approved by the Laboratory Animal Management and Ethics Committee of Fujian Medical University with approved number FJMU IACUC 2021-0298 and

were performed in accordance with the "China Guide for the Protection and Use of Laboratory Animals".

ADDITIONAL INFORMATION

Supplementary information contains supplementary figures 1-8 and legends.

REFERENCES

Bao YW, Yuan Y, Chen JH, et al. 2018. Kidney disease models: tools to identify mechanisms and potential therapeutic targets. *Zool Res*, **39**(2): 72-86.

Baudoux T, Jadot I, Declèves AE, et al. 2022. Experimental Aristolochic Acid Nephropathy: A Relevant Model to Study AKI-to-CKD Transition. *Front Med (Lausanne)*, **9**: 822870.

Bellamri M, Brandt K, Brown CV, et al. 2021. Cytotoxicity and genotoxicity of the carcinogen aristolochic acid I (AA-I) in human bladder RT4 cells. *Arch Toxicol*, **95**(6): 2189-2199.

Chen C, Xie J, Chen Z, et al. 2025. Role of Z-DNA Binding Protein 1 Sensing Mitochondrial Z-DNA and Triggering Necroptosis in Oxalate-Induced Acute Kidney Injury. *J Am Soc Nephrol*, **36**(3): 361-377.

Chen J, Luo P, Wang C, et al. 2022. Integrated single-cell transcriptomics and proteomics reveal cellular-specific responses and microenvironment remodeling in aristolochic acid nephropathy. *JCI Insight*, **7**(16).

Chesnaye NC, Carrero JJ, Hecking M, et al. 2024. Differences in the epidemiology, management and outcomes of kidney disease in men and women. *Nat Rev Nephrol*, **20**(1): 7-20.

Debelle FD, Vanherweghem JL, Nortier JL. 2008. Aristolochic acid nephropathy: a worldwide problem. *Kidney Int*, **74**(2): 158-169.

Gökmen MR, Cosyns JP, Arlt VM, et al. 2013. The epidemiology, diagnosis, and management of aristolochic acid nephropathy: a narrative review. *Ann Intern Med*, **158**(6): 469-477.

Ha SC, Kim D, Hwang HY, et al. 2008. The crystal structure of the second Z-DNA binding domain of human DAI (ZBP1) in complex with Z-DNA reveals an unusual binding mode to Z-DNA. *Proc Natl Acad Sci U S A*, **105**(52): 20671-20676.

Han J, Xian Z, Zhang Y, et al. 2019. Systematic Overview of Aristolochic Acids: Nephrotoxicity, Carcinogenicity, and Underlying Mechanisms. *Front Pharmacol*, **10**: 648.

Jelaković B, Vuković Lela I, Karanović S, et al. 2015. Chronic dietary exposure to aristolochic acid and kidney function in native farmers from a Croatian endemic area and Bosnian immigrants. *Clin J Am Soc Nephrol*, **10**(2): 215-223.

Ji H, Hu J, Zhang G, et al. 2021. Aristolochic acid nephropathy: A scientometric analysis of literature published from 1971 to 2019. *Medicine (Baltimore)*, **100**(27): e26510.

Jiao H, Wachsmuth L, Kumari S, et al. 2020. Z-nucleic-acid sensing triggers ZBP1-dependent necroptosis and inflammation. *Nature*, **580**(7803): 391-395.

Kiliś-Pstrusińska K & Wiela-Hojeńska A. 2021. Nephrotoxicity of Herbal Products in Europe-A Review of an Underestimated Problem. *Int J Mol Sci*, **22**(8).

Koerner L, Wachsmuth L, Kumari S, et al. 2024. ZBP1 causes inflammation by inducing RIPK3-mediated necroptosis and RIPK1 kinase activity-independent apoptosis. *Cell Death Differ*, **31**(7): 938-953.

Kuriakose T & Kanneganti TD. 2018. ZBP1: Innate Sensor Regulating Cell Death and Inflammation. *Trends Immunol*, **39**(2): 123-134.
Lai K, Wang J, Lin S, et al. 2024. Sensing of mitochondrial DNA by ZBP1 promotes RIPK3-mediated necroptosis and ferroptosis in response to diquat poisoning. *Cell Death Differ*, **31**(5): 635-650.
Lei Y, Vanportfliet JJ, Chen YF, et al. 2023. Cooperative sensing of mitochondrial DNA by ZBP1 and cGAS promotes cardiotoxicity. *Cell*, **186**(14): 3013-3032.e3022.
Lin J, Kumari S, Kim C, et al. 2016. RIPK1 counteracts ZBP1-mediated necroptosis to inhibit inflammation. *Nature*, **540**(7631): 124-128.
Liu X, Wu J, Wang J, et al. 2020. Mitochondrial dysfunction is involved in aristolochic acid I-induced apoptosis in renal proximal tubular epithelial cells. *Hum Exp Toxicol*, **39**(5): 673-682.
Long T, Lu Y, Ma Y, et al. 2025. Condensation of cellular prion protein promotes renal fibrosis through the TBK1-IRF3 signaling axis. *Sci Transl Med*, **17**(794): eadj9095.
Maelfait J, Liverpool L, Bridgeman A, et al. 2017. Sensing of viral and endogenous RNA by ZBP1/DAI induces necroptosis. *Embo j*, **36**(17): 2529-2543.
Maelfait J & Rehwinkel J. 2023. The Z-nucleic acid sensor ZBP1 in health and disease. *J Exp Med*, **220**(8).
Miao J, Zhu H, Wang J, et al. 2024. Experimental models for preclinical research in kidney disease. *Zool Res*, **45**(5): 1161-1174.
Mishra S, Dey AA, Kesavardhana S. 2025. Z-Nucleic Acid Sensing and Activation of ZBP1 in Cellular Physiology and Disease Pathogenesis. *Immunol Rev*, **329**(1): e13437.
Muendlein HI, Connolly WM, Magri Z, et al. 2021. ZBP1 promotes LPS-induced cell death and IL-1β release via RHIM-mediated interactions with RIPK1. *Nat Commun*, **12**(1): 86.
Newton K, Wickliffe KE, Maltzman A, et al. 2016. RIPK1 inhibits ZBP1-driven necroptosis during development. *Nature*, **540**(7631): 129-133.
Ofengeim D & Yuan J. 2013. Regulation of RIP1 kinase signalling at the crossroads of inflammation and cell death. *Nat Rev Mol Cell Biol*, **14**(11): 727-736.
Patidar KR, Ma AT, Juanola A, et al. 2025. Global epidemiology of acute kidney injury in hospitalised patients with decompensated cirrhosis: the International Club of Ascites GLOBAL AKI prospective, multicentre, cohort study. *Lancet Gastroenterol Hepatol*, **10**(5): 418-430.
Pozdzik AA, Salmon IJ, Debelle FD, et al. 2008. Aristolochic acid induces proximal tubule apoptosis and epithelial to mesenchymal transformation. *Kidney Int*, **73**(5): 595-607.
Rodriguez DA, Quarato G, Liedmann S, et al. 2022. Caspase-8 and FADD prevent spontaneous ZBP1 expression and necroptosis. *Proc Natl Acad Sci U S A*, **119**(41): e2207240119.
Sasaki K, Terker AS, Tang J, et al. 2022. Macrophage interferon regulatory factor 4 deletion ameliorates aristolochic acid nephropathy via reduced migration and increased apoptosis. *JCI Insight*, **7**(4).
Sborchia M, De Prez EG, Antoine MH, et al. 2019. The impact of p53 on aristolochic acid I-induced nephrotoxicity and DNA damage in vivo and in vitro. *Arch Toxicol*, **93**(11): 3345-3366.
Shen QQ, Wang JJ, Roy D, et al. 2020. Organic anion transporter 1 and 3 contribute to traditional Chinese medicine-induced nephrotoxicity. *Chin J Nat Med*, **18**(3): 196-205.
Solon M, Ge N, Hambro S, et al. 2024. ZBP1 and TRIF trigger lethal necroptosis in mice lacking caspase-8 and TNFR1. *Cell Death Differ*, **31**(5): 672-682.
Takaoka A, Wang Z, Choi MK, et al. 2007. DAI (DLM-1/ZBP1) is a cytosolic DNA sensor and an activator of innate immune response. *Nature*, **448**(7152): 501-505.
Vanherweghem JL, Depierreux M, Tielemans C, et al. 1993. Rapidly progressive interstitial renal fibrosis in young women: association with slimming regimen including Chinese herbs. *Lancet*, **341**(8842): 387-391.

Wang L, Shao Z, Wang N, et al. 2024. Receptor-interacting protein kinase 1 confers autophagic promotion of gasdermin E-mediated pyroptosis in aristolochic acid-induced acute kidney injury. *Ecotoxicol Environ Saf*, **284**: 116944.

Wu TK, Wei CW, Pan YR, et al. 2015. Vitamin C attenuates the toxic effect of aristolochic acid on renal tubular cells via decreasing oxidative stress‐mediated cell death pathways. *Mol Med Rep*, **12**(4): 6086-6092.

Xie XC, Zhao N, Xu QH, et al. 2017. Relaxin attenuates aristolochic acid induced human tubular epithelial cell apoptosis in vitro by activation of the PI3K/Akt signaling pathway. *Apoptosis*, **22**(6): 769-776.

Xu Y, Ma H, Shao J, et al. 2015. A Role for Tubular Necroptosis in Cisplatin-Induced AKI. *J Am Soc Nephrol*, **26**(11): 2647-2658.

Xue X, Gong LK, Maeda K, et al. 2011. Critical role of organic anion transporters 1 and 3 in kidney accumulation and toxicity of aristolochic acid I. *Mol Pharm*, **8**(6): 2183-2192.

Yang B, Xie Y, Guo M, et al. 2018. Nephrotoxicity and Chinese Herbal Medicine. *Clin J Am Soc Nephrol*, **13**(10): 1605-1611.

Yang D, Liang Y, Zhao S, et al. 2020. ZBP1 mediates interferon-induced necroptosis. *Cell Mol Immunol*, **17**(4): 356-368.

Yuan J & Ofengeim D. 2024. A guide to cell death pathways. *Nat Rev Mol Cell Biol*, **25**(5): 379-395.

Zhou L, Fu P, Huang XR, et al. 2010. Activation of p53 promotes renal injury in acute aristolochic acid nephropathy. *J Am Soc Nephrol*, **21**(1): 31-41.

Zhou Y, Cui R, Zhang M, et al. 2024. Mitochondrial uptake of aristolactam I plays a critical role in its toxicity. *Toxicol Lett*, **394**: 76-91.

FIGURE and FIGURE LEGENDS

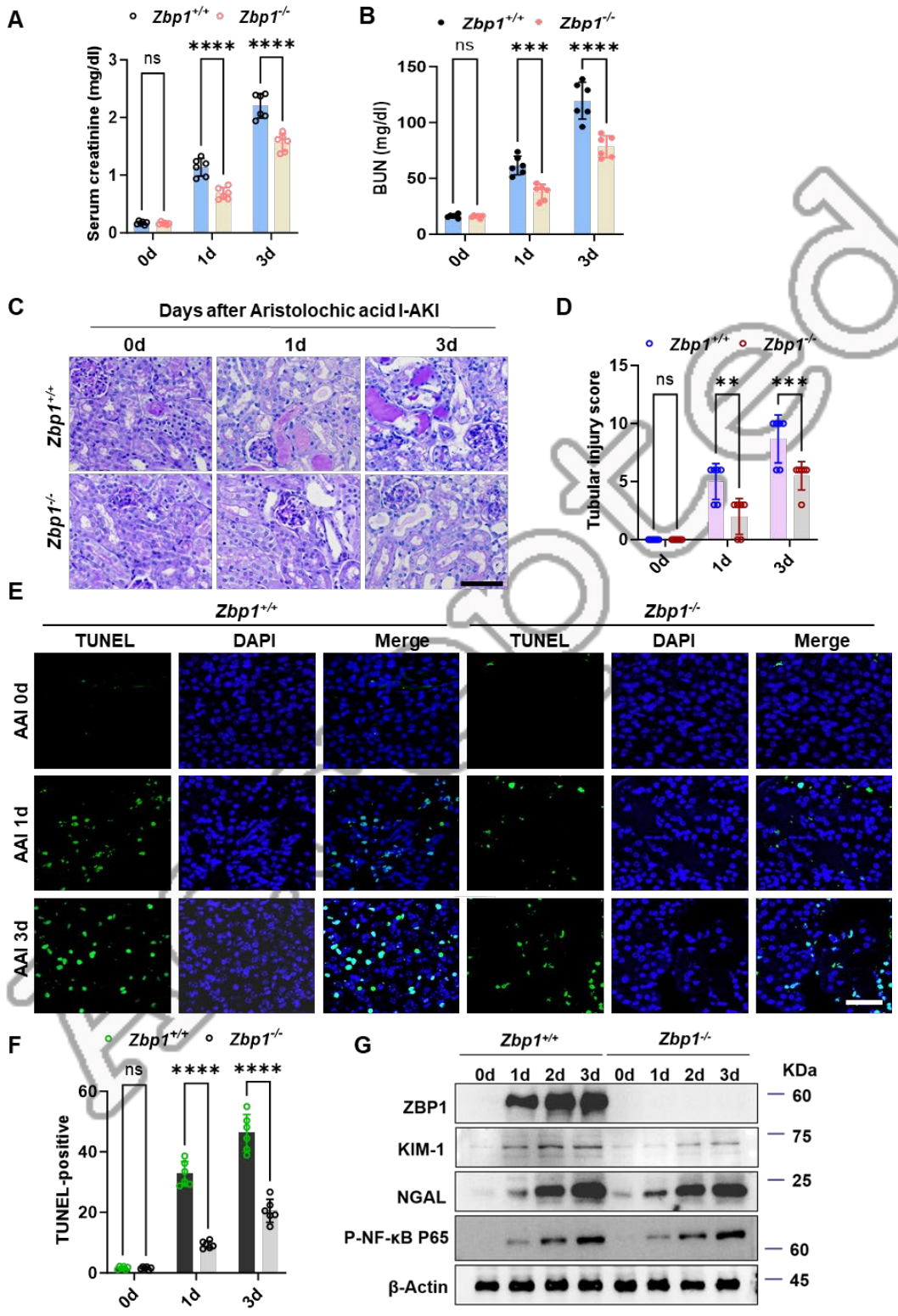

Figure 1. ZBP1 deficiency protects against acute kidney injury induced by aristolochic

acid I (AAI).

A: Serum creatinine levels in *Zbp1*$^{+/+}$ and *Zbp1*$^{-/-}$ mice at baseline (0 day), and 1 or 3 days after a single intraperitoneal injection of AAI (10 mg/kg), (n = 6 mice/group).

B: Blood urea nitrogen (BUN) levels measured in *Zbp1*$^{+/+}$ and *Zbp1*$^{-/-}$ mice at the indicated time points (n = 6 per group).

C: Representative periodic acid–Schiff (PAS) staining of kidney sections from *Zbp1*$^{+/+}$ and *Zbp1*$^{-/-}$ mice at 0, 1, and 3 days after AAI administration. Scale bar, 50 μm.

D: Tubular injury scores from PAS-stained kidney sections indicate significant attenuation of injury in *Zbp1*$^{-/-}$ mice (n = 5 per group).

E: Representative TUNEL staining of renal cortical sections from *Zbp1*$^{+/+}$ and *Zbp1*$^{-/-}$ mice at 0, 1, and 3 days after AAI treatment. TUNEL (green), DAPI (blue). Scale bar, 50 μm.

F: Quantification of TUNEL-positive nuclei shows significantly reduced tubular cell death in *Zbp1*$^{-/-}$ kidneys at 1 and 3 days after AAI administration (n = 6 per group).

G: Western blot analysis of whole-kidney lysates from *Zbp1*$^{+/+}$ and *Zbp1*$^{-/-}$ mice at 0-, 1-, and 3-days post-AAI injury. ZBP1, KIM-1, and NGAL were induced in *Zbp1*$^{+/+}$ kidneys, whereas NF-κB activation (p65 phosphorylation) showed no difference between groups. β-Actin served as a loading control.

Data are shown as mean ± SD. $*P < 0.05$, $**P < 0.01$, $***P < 0.001$.

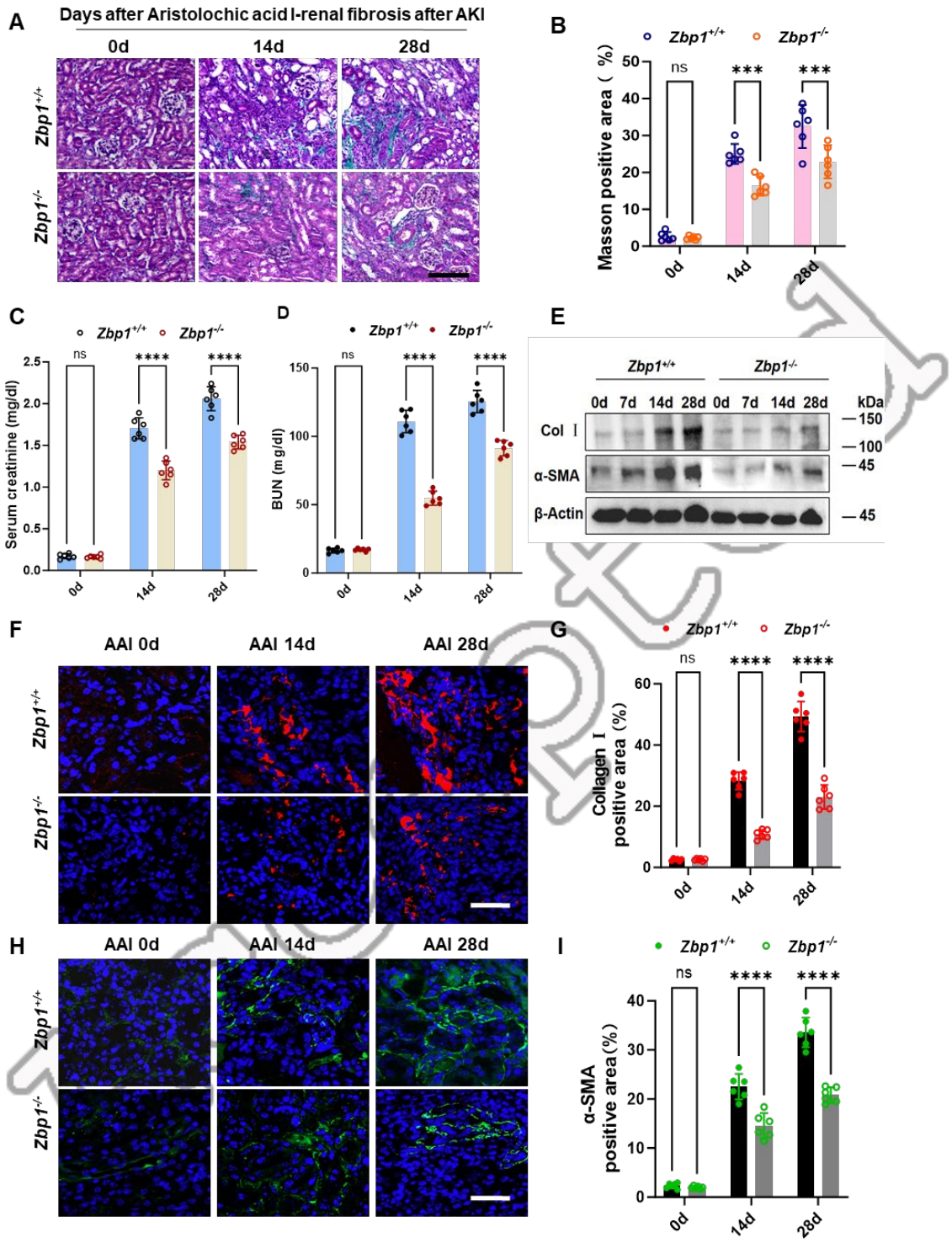

Figure 2. ZBP1 deficiency attenuates renal fibrosis following AAI exposure.

A: Representative Masson's trichrome staining showing reduced tubulointerstitial injury and fibrotic progression in *Zbp1*$^{+/+}$ and *Zbp1*$^{-/-}$ kidneys at 0, 14, and 28 days after AAI

administration. Scale bar, 50 μm.

B: Quantification of Masson's trichrome–positive area (% of total area).

C: Serum creatinine levels measured at the indicated time points (n = 6 per group).

D: Blood urea nitrogen (BUN) levels measured at the indicated time points (n = 6 per group).

E: Western blot analysis of collagen I and α-SMA expression in whole-kidney lysates from *Zbp1*$^{+/+}$ and *Zbp1*$^{-/-}$ mice at 0, 7, 14, and 28 days following AAI exposure. β-actin served as a loading control.

F: Representative immunofluorescence images of collagen I (red) deposition in renal sections. Scale bar, 50 μm.

G: Quantification of collagen I–positive area.

H: Immunofluorescence staining of α-smooth muscle actin (α-SMA, green). Scale bar, 50 μm.

I: Quantification of α-SMA–positive area.

Data are presented as mean ± SD. ns, not significant; **P < 0.05; **P < 0.01; ***P < 0.001; ****P < 0.0001*.

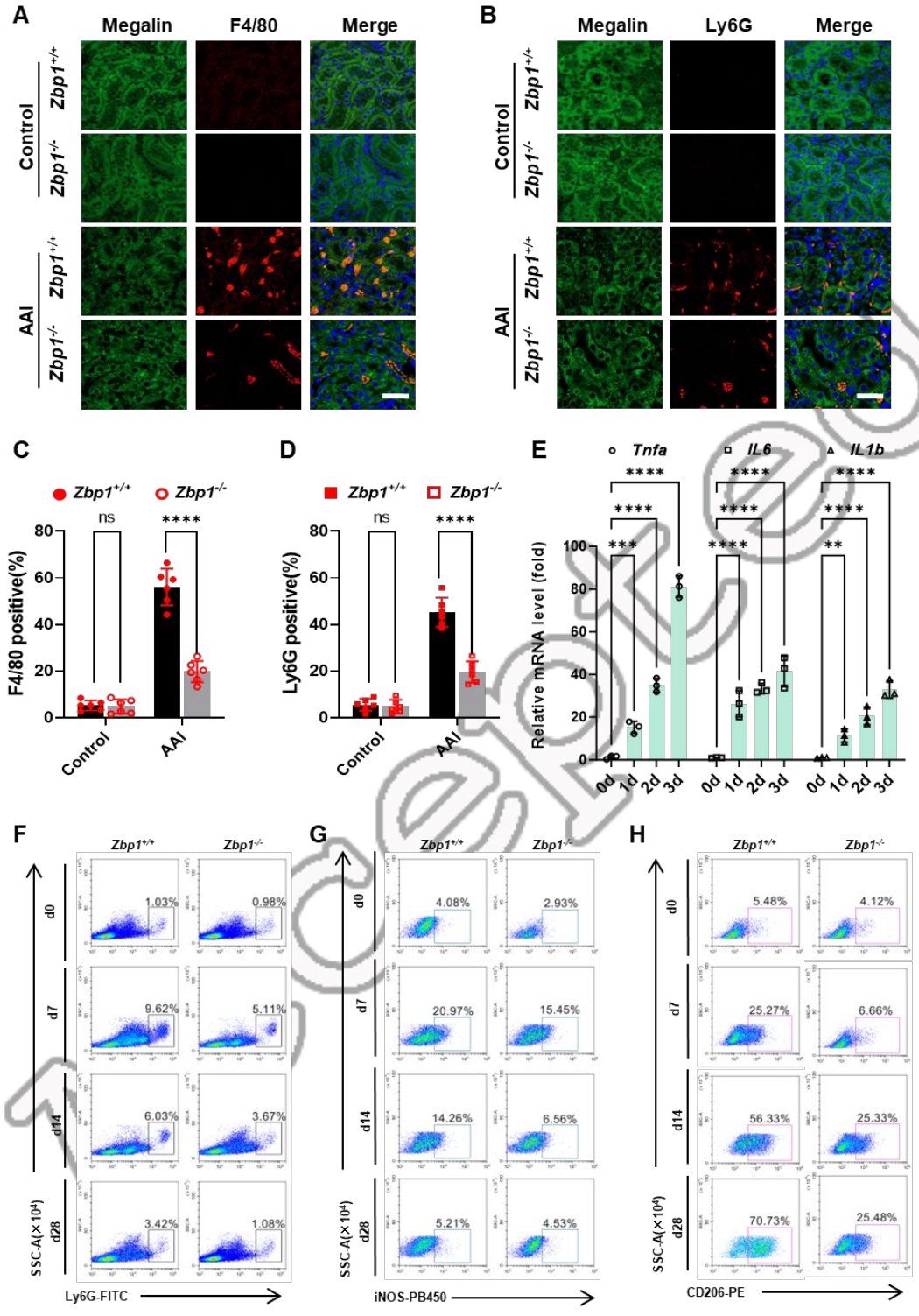

Figure 3. ZBP1 promotes immune cell infiltration and inflammatory cytokine expression in AAI nephropathy.

A: Immunofluorescence staining of kidney sections from *Zbp1*$^{+/+}$ and *Zbp1*$^{-/-}$ mice treated with vehicle or AAI for 7 days showing marked accumulation of F4/80^{+} macrophages and Ly6G^{+} neutrophils in *Zbp1*$^{+/+}$ kidneys, which was substantially reduced in *Zbp1*$^{-/-}$ kidneys.

B: Quantification of F4/80^{+} and Ly6G^{+} staining areas demonstrating significantly lower immune cell infiltration in *Zbp1*$^{-/-}$ kidneys after AAI exposure.

C: qRT-PCR analysis of renal mRNA expression of TNF-α, IL-6, and IL-1β at 1, 3, and 7 days following AAI injection.

D: Flow cytometric analysis of kidney single-cell suspensions at the indicated time points post-AAI injection.

E: Frequencies of Ly6G^{+} neutrophils and iNOS^{+} M1-like macrophages peaked at day 7 in *Zbp1*$^{+/+}$ kidneys and were reduced in *Zbp1*$^{-/-}$ kidneys.

F: CD206^{+} M2-like macrophages progressively increased over time in both genotypes, but this expansion was attenuated in *Zbp1*$^{-/-}$ kidneys.

Data are presented as mean ± SD (n = 5–6 mice per group). Scale bars, 100 μm. ns, not significant; *$P < 0.05$; **$P < 0.01$; ***$P < 0.001$.

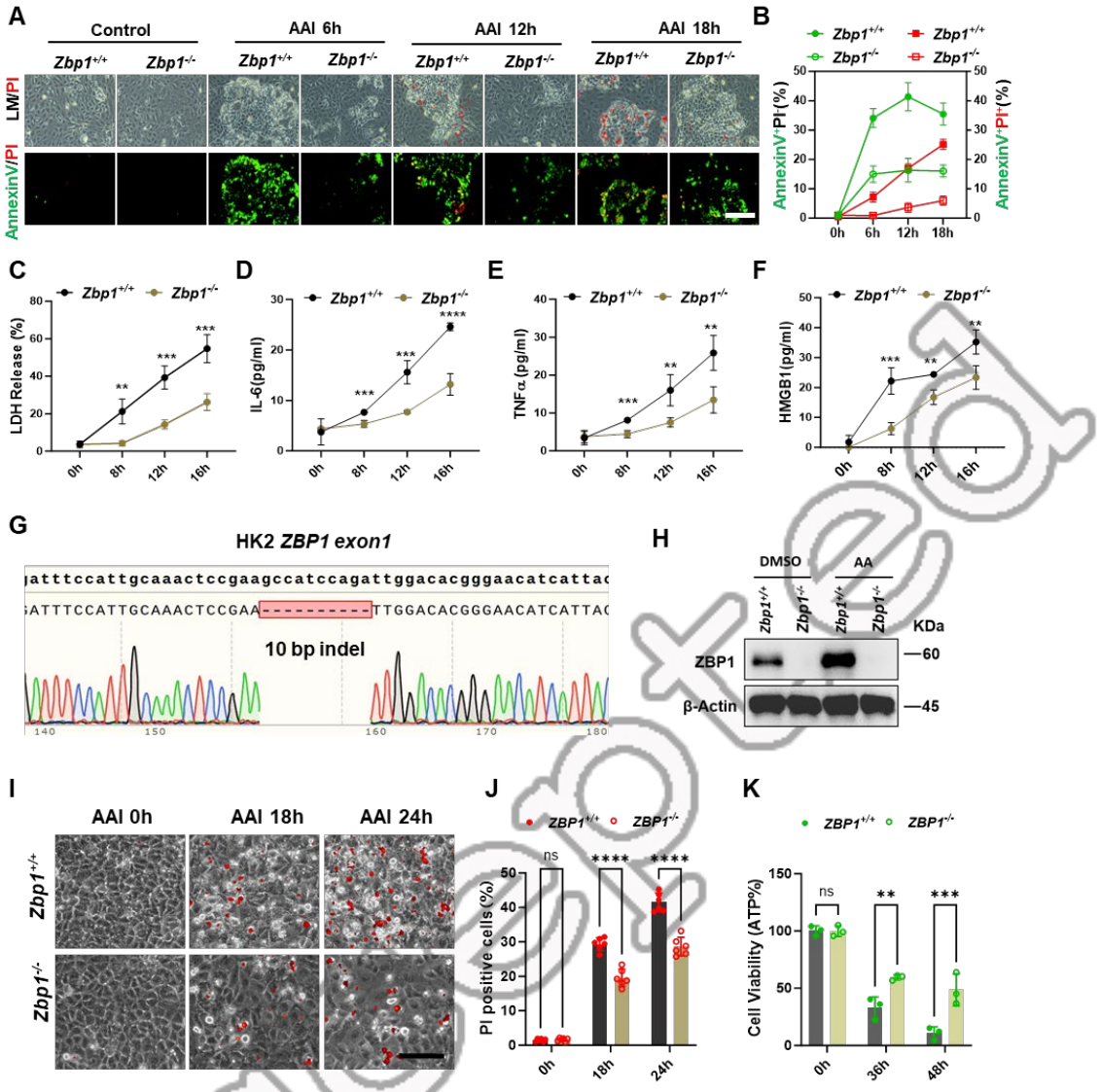

Figure 4. ZBP1 promotes tubular cell death and inflammatory responses upon AAI exposure *in vitro*.

A: Representative images of primary tubular epithelial cells (TECs) isolated from *Zbp1*$^{+/+}$ and *Zbp1*$^{-/-}$ mice and stained with Annexin V/PI following 0, 6, 12, and 18 hours of AAI exposure, showing progression from apoptosis to secondary necrosis. Scale bar, 50 μm.

B: Quantification of Annexin V^+/PI^- and Annexin V^+/PI^+ cell populations from panel A.

C: ELISA quantification of LDH release in the supernatants of AAI-treated TECs over time.

D: ELISA quantification of IL-6 levels in TEC supernatants.

E: ELISA quantification of TNF-α levels in TEC supernatants.

F: ELISA quantification of HMGB1 release in TEC supernatants.

G: Sanger sequencing confirming CRISPR/Cas9-mediated *ZBP1* exon 1 editing in HK-2 cells, introducing a 10 bp indel.

H: Western blot confirming ZBP1 knockout in HK-2 cells after 18 hours of AAI treatment.

I: Live-cell imaging of PI-positive cells in wild-type (WT) and *ZBP1*$^{-/-}$ HK-2 cells treated with AAI for 0, 18, or 24 hours. Scale bar, 100 μm.

J: Quantification of PI-positive cells.

K: ATP-based viability assay of WT and *ZBP1*$^{-/-}$ HK-2 cells treated with AAI for 36 and 48 hours.

Data are presented as mean ± SD. ns, not significant; *$P < 0.05$; **$P < 0.01$; ***$P < 0.001$; ****$P < 0.0001$.

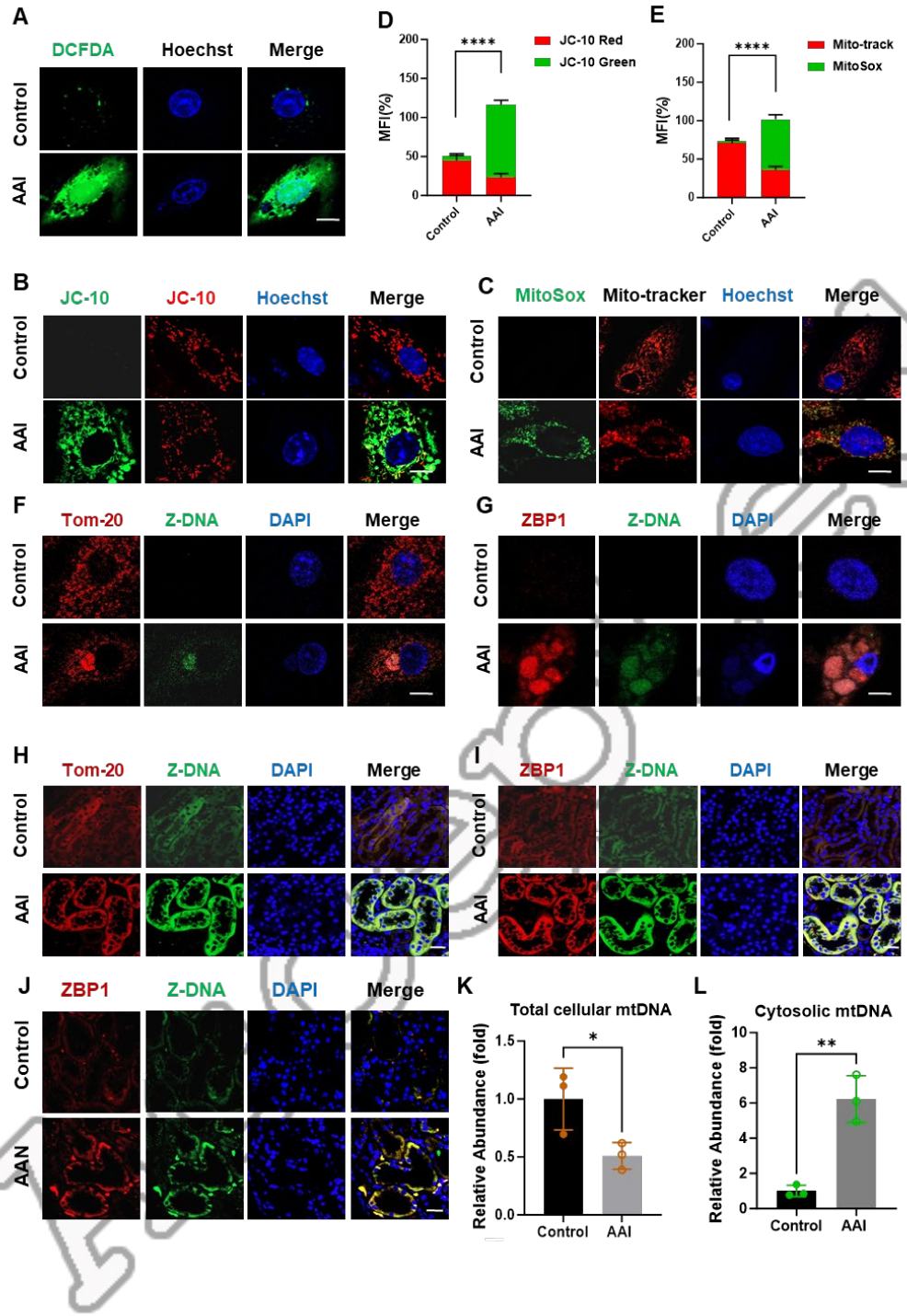

Figure 5. AAI-induced mitochondrial stress and Z-form mitochondrial DNA formation in tubular epithelial cells.

A: DCFDA staining showing ROS accumulation in AAI-treated TECs.

B: JC-10 staining showing mitochondrial membrane potential loss following AAI exposure.

C: MitoSOX staining showing mitochondrial superoxide production in TECs after AAI treatment.

D: Quantification of JC-10 red/green fluorescence ratio.

E: Quantification of MitoSOX-positive cells.

F: Confocal microscopy showing Tom20-labeled mitochondrial network and Z-DNA formation in TECs after AAI treatment. Scale bar, 10 μm.

G: Colocalization of ZBP1 and Z-DNA in the cytoplasm of AAI-treated TECs. Scale bar, 10 μm.

H: Immunofluorescence staining showing colocalization of ZBP1, Tom20, and Z-DNA in tubular cells from kidneys after AAI exposure. Scale bar, 10 μm.

I: Quantification of colocalization in kidney sections.

J: Representative immunofluorescence images showing similar ZBP1–Tom20–Z-DNA colocalization in human kidney biopsy samples from patients with AAN. Scale bar, 60 μm.

K: qPCR quantification of total mitochondrial DNA in TECs after AAI treatment.

L: qPCR quantification of cytosolic mtDNA from TECs after AAI exposure.

Data are mean ± SD. *$P < 0.05$, **$P < 0.01$, ***$P < 0.001$, ****$P < 0.0001$.

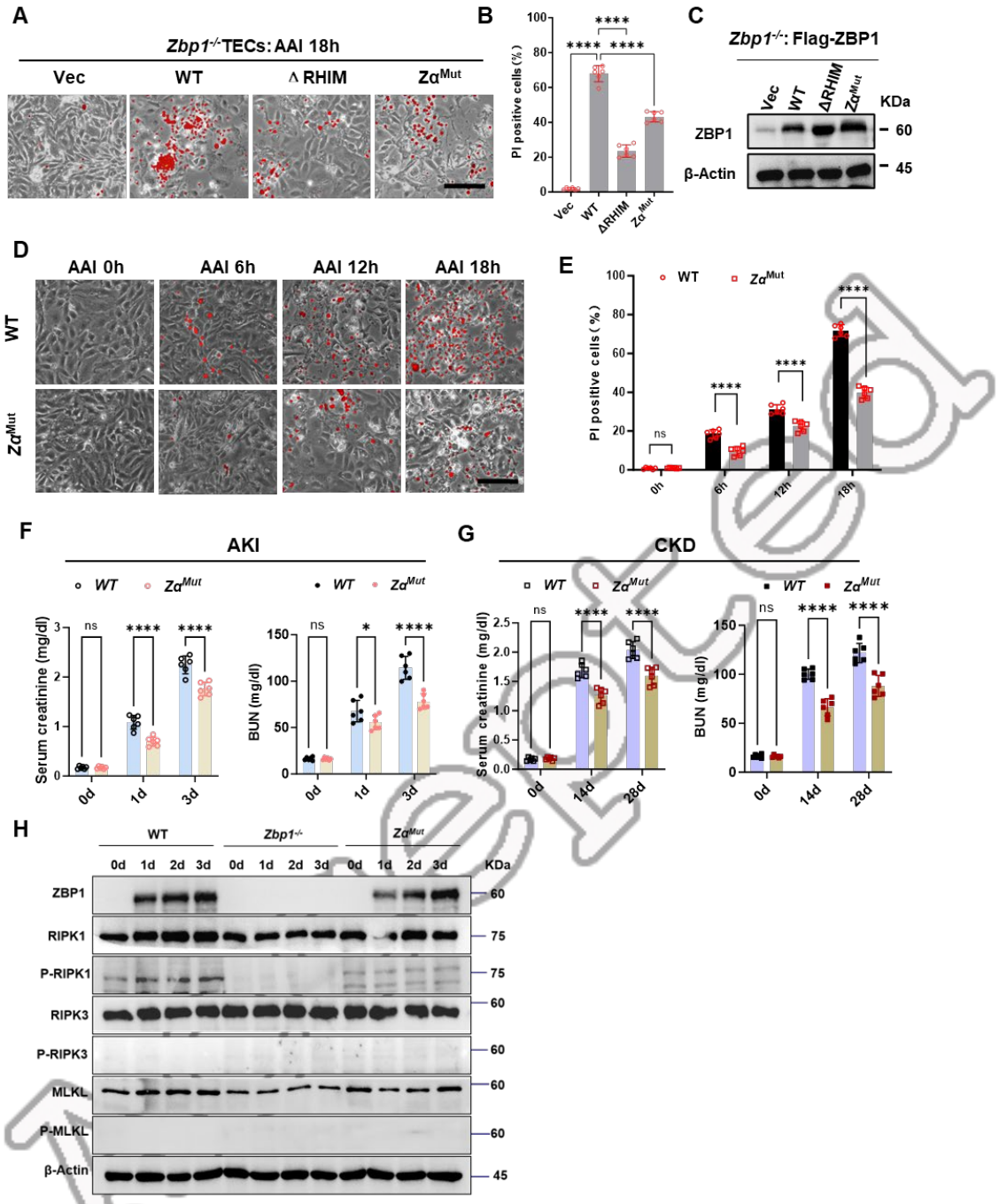

Figure 6. Zα domain of ZBP1 is essential for sensing Z-mtDNA and mediating tubular death and nephropathy.

A: Representative images of PI-positive cells in *Zbp1*$^{-/-}$ TECs reconstituted with Flag-tagged ZBP1 wild-type (WT), ΔRHIM, or Zα^{Mut} constructs following AAI treatment. Scale bar, 100 μm.

B: Quantification of PI-positive cells.

C: Western blot confirming ZBP1 expression.

D: Representative images of time-lapse PI staining in wild-type (WT) and $Z\alpha^{Mut}$ TECs at indicated time points after AAI exposure. Scale bar, 100 μm.

E: Quantification of time-lapse PI staining.

F: Serum creatinine levels in WT and $Z\alpha^{Mut}$ mice at indicated time points after AAI exposure (n = 6 per group).

G: BUN levels in WT and $Z\alpha^{Mut}$ mice at indicated time points after AAI exposure (n = 6 per group).

H: Western blot analysis of renal tissues from WT, $Zbp1^{-/-}$, and $Z\alpha^{Mut}$ mice showing ZBP1, RIPK1/RIPK3/MLKL, and their phosphorylated forms at indicated time points post-AAI treatment.

Data are mean ± SD. *$P < 0.05$, **$P < 0.01$, ***$P < 0.001$, ****$P < 0.0001$.

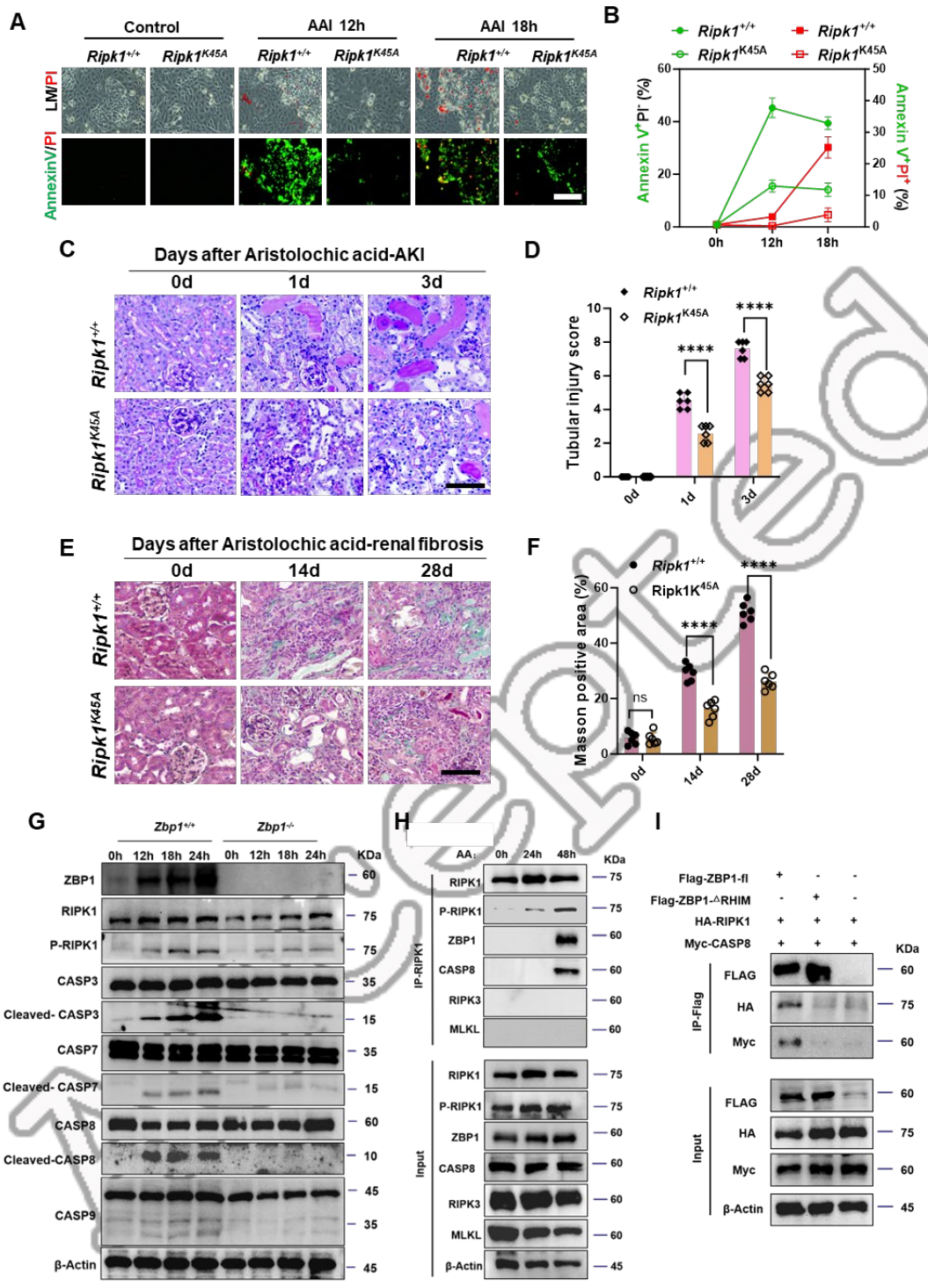

Figure 7. ZBP1 mediates AAI-induced tubular cell apoptosis via RIPK1 scaffolding function.

Science Press
ZR Zoological Research

A: Representative images of primary tubular epithelial cells (TECs) isolated from wild-type (*Ripk1*$^{+/+}$) and *Ripk1*^{K45A} mice and stained with Annexin V/PI following 0, 12, and 18 hours of AAI exposure. Scale bar, 50 μm.

B: Quantification of Annexin V^+/PI^- and Annexin V^+/PI^+ cell populations from panel A.

C: Representative PAS-stained kidney sections from *Ripk1*$^{+/+}$ and *Ripk1*^{K45A} mice at 0, 1, and 3 days after AAI administration. Scale bar, 100 μm.

D: Quantification of PAS staining.

E: Representative Masson's trichrome staining of kidneys from *Ripk1*$^{+/+}$ and *Ripk1*^{K45A} mice at 0, 14, and 28 days after AAI administration. Scale bar, 60 μm.

F: Quantification of Masson's trichrome staining.

G: Western blot showing expression of RIPK1/pRIPK, caspase-3, -7, -8, -9, and cleaved fragments in TECs from WT or *Zbp1*$^{-/-}$ mice treated with AAI for 0–24 h.

H: Immunoprecipitation of RIPK1 in TECs treated with AAI for 0, 24, 48 h shows time-dependent interaction with ZBP1 and Caspase-8.

I: Co-immunoprecipitation of FLAG-ZBP1-FL or (L) FLAG-ZBP1-ΔRHIM with HA-RIPK1 or Myc-caspase-8 in HEK293T cells treated with AAI for the indicated times. Data are shown as mean ± SD. *$P < 0.05$, **$P < 0.01$, ***$P < 0.001$, ****$P < 0.0001$.

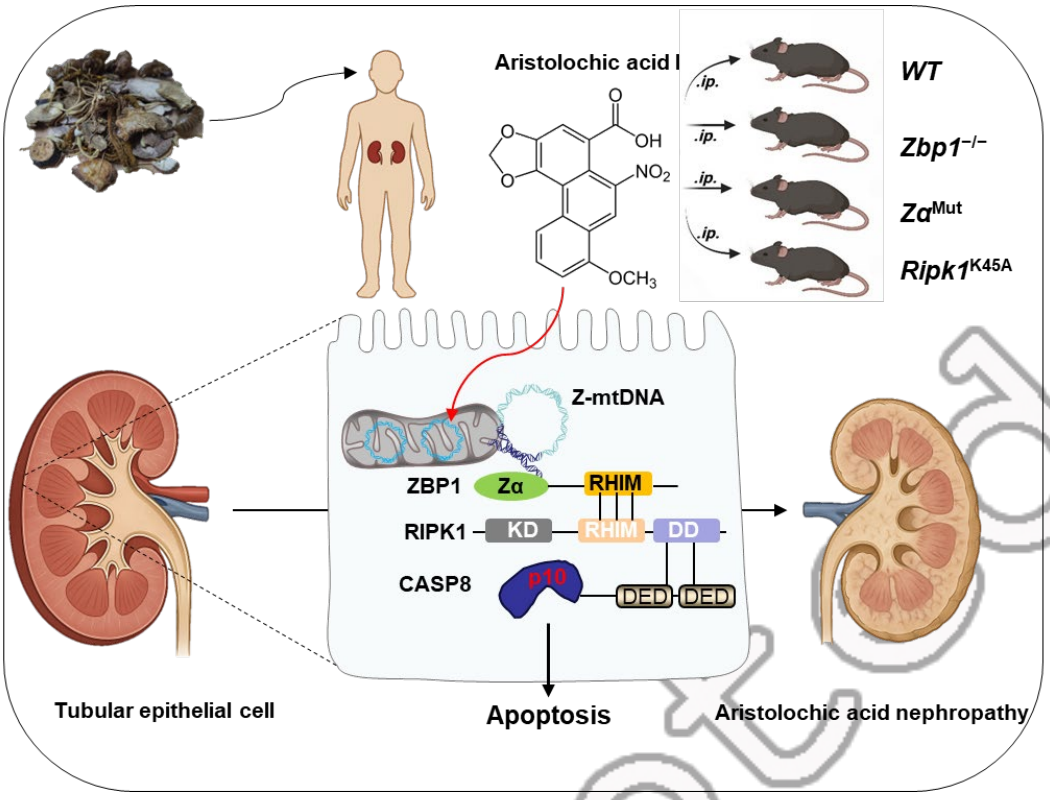

Figure 8. Schematic diagram of this study

ZBP1 senses mitochondrial Z-DNA to trigger RIPK1–caspase-dependent tubular apoptosis in aristolochic acid nephropathy (AAN). Part of the diagram was created using BioRender (www.biorender.com).

ZBP1 促进 RIPK1 依赖的凋亡在马兜铃酸肾病中的作用

邹臻寰 [1,2,3,#], 叶铿 [1,2,3,#], 陈锋斌 [4], 林孔文 [1,2,3], 宋彦锟 [5], 李国平 [5], 陈财铭 [1,2,3], 王宇佳 [1,2,3], 马华彬 [2,6,*], 许艳芳 [1,2,3,6,*]

[1]福建医科大学附属第一医院肾内科，血液净化研究中心，福建 福州 350005

[2]福建医科大学附属第一医院代谢性慢性肾脏病临床医学研究中心，福建 福州 350005

[3]福建医科大学附属第一医院滨海院区国家区域医疗中心肾内科，福建 福州 350212

[4]福建医科大学附属第一医院中医科，福建 福州 350005

[5]福建医科大学附属第一医院病理科，福建 福州 350005

[6]福建医科大学附属第一医院中心实验室，福建 福州 350005

[#]共同第一作者：邹臻寰，叶铿

[*]通讯作者：

许艳芳，邮箱：xuyanfang99@hotmail.com；马华彬，邮箱：mahuabin@fjmu.edu.cn

Science Press ZR Zoological Research

摘要

马兜铃酸肾病（aristolochic acid nephropathy，AAN）是一类进展性肾脏疾病，以急性肾小管损伤和间质纤维化为主要特征，可最终发展为终末期肾病（ESRD）。尽管已实施严格管控，但由于马兜铃酸仍存在于部分传统草药中，其带来的全球健康威胁依然严峻。线粒体介导的凋亡是AA诱导肾小管上皮细胞（TEC）损伤的典型机制，但其上游调控环节尚未阐明。本研究鉴定了Z-DNA结合蛋白1（ZBP1）在AA诱导的肾损伤中的关键作用。利用*Zbp1*基因敲除（*Zbp1*$^{-/-}$）和Zα结构域突变（*Zα*^{Mut}）小鼠模型，我们发现缺失ZBP1或其Z型核酸识别能力可显著缓解AA导致的肾功能障碍、凋亡与炎症反应。机制研究显示，马兜铃酸I（AAI）诱导线粒体氧化应激及线粒体DNA（mtDNA）外泄，外泄的mtDNA呈现Z构象并被ZBP1识别。ZBP1结合随后促进其与RIPK1的RHIM依赖性相互作用，进而激活caspase-8，引发凋亡。值得注意的是，ZBP1介导的细胞死亡可以通过RIPK1激酶抑制剂或激酶缺陷突变阻断，但不受*Ripk3*或*Mlkl*敲除影响，提示其机制区别于经典的RIPK3/MLKL依赖性程序性坏死。上述发现揭示了ZBP1–RIPK1–caspase-8信号轴驱动AAN中非典型凋亡过程，并提示靶向该通路可能成为治疗肾毒性肾损伤的新策略。

关键词

马兜铃酸肾病；凋亡；线粒体；ZBP1；Z-DNA